Naval Research Laboratory

Washington, DC 20375-5320

NRL/MR/5520--18-9769

Distributed Spectral Monitoring for Emitter Localization

Matthew Dillon
Joseph A. Molnar
Andrew Robertson

Networks and Communications Branch
Information and Technology Division

Er-Hsien (Frank) Fu

KEYW Corporation
Hanover, MD

February 12, 2018

REPORT DOCUMENTATION PAGE

Form Approved
OMB No. 0704-0188

1. REPORT DATE *(DD-MM-YYYY)*	**2. REPORT TYPE**	**3. DATES COVERED** *(From - To)*
12-02-2018	Memorandum Report	07-03-2015 - 07-03-2017

4. TITLE AND SUBTITLE

Distributed Spectral Monitoring For Emitter Localization

5a. CONTRACT NUMBER

5b. GRANT NUMBER

5c. PROGRAM ELEMENT NUMBER

6. AUTHOR(S)

Matthew Dillon, Joseph A. Molnar, Andrew Robertson and Er-Hsien (Frank) Fu*

5d. PROJECT NUMBER
55-6875-07

5e. TASK NUMBER

5f. WORK UNIT NUMBER
6875

7. PERFORMING ORGANIZATION NAME(S) AND ADDRESS(ES)

Naval Research Laboratory
4555 Overlook Ave, SW
Washington, DC 20375-5320

8. PERFORMING ORGANIZATION REPORT NUMBER

NRL/MR/5520--18-9769

9. SPONSORING / MONITORING AGENCY NAME(S) AND ADDRESS(ES)

Naval Research Laboratory
4555 Overlook Avenue, SW
Washington, DC 20375-5320

10. SPONSOR / MONITOR'S ACRONYM(S)

NRL

11. SPONSOR / MONITOR'S REPORT NUMBER(S)

12. DISTRIBUTION / AVAILABILITY STATEMENT

DISTRIBUTION STATEMENT A: Approved for public release; distribution is unlimited.

13. SUPPLEMENTARY NOTES

*KEYW Corporation, Hanover, MD

14. ABSTRACT

The geolocation of RF emitters is an important capability for DSA (dynamic spectrum access) enabled sensor networks. The purpose of this report is to present research and application of the various localization techniques in a DSA sensor network. The results of the research are presented through simulation of localization algorithms, emulation of a network on a wireless RF environment emulator, and field tests. The results of the various tests in both the lab and field are obtained and analyzed to determine whether the field tests and emulation results correspond to the theoretical simulations.

15. SUBJECT TERMS

Blind localization, spectral monitoring, dynamic-spectrum-access (DSA), universal software radio peripheral (USRP), software defined radio, cognitive radio, wireless channel emulation

16. SECURITY CLASSIFICATION OF:			**17. LIMITATION OF ABSTRACT**	**18. NUMBER OF PAGES**	**19a. NAME OF RESPONSIBLE PERSON**
a. REPORT	**b. ABSTRACT**	**c. THIS PAGE**			Joseph A. Molnar
Unclassified Unlimited	Unclassified Unlimited	Unclassified Unlimited	SAR	24	**19b. TELEPHONE NUMBER** *(include area code)* (202) 767-0327

Standard Form 298 (Rev. 8-98)
Prescribed by ANSI Std. Z39.18

This page intentionally left blank.

CONTENTS

This page intentionally left blank.

DISTRIBUTED SPECTRAL MONITORING FOR EMITTER LOCALIZATION

1. BACKGROUND

The purpose of this effort is to investigate technologies needed to develop a network of sensors with spectrum monitoring capabilities and to provide a correlated perspective of extraneous emitters. This assessment of the environment can further be used to adjust spectral policy for a network, and optimize network throughput.

The geolocation of RF emitters is an important capability for spectrum situational awareness. Several techniques exist to track the position of RF emitters. There are two main classes of localization techniques, and the technique to use will depend on the information available with the emitter. The first class of techniques assumes that a priori knowledge is available for the emitter, such as the emitter and sensors being time synchronized and knowing information about its waveform and transmit power. Knowing this information, techniques such as using the time of arrival (TOA) to determine the distance between the emitter and sensors [6] may be employed. The other class of localization techniques is used when there is no *a priori* knowledge available (blind localization). In this case, the sensors must use information such as the received signal strength indicator (RSSI) of the spectrum of interest and IQ samples and correlate the information to estimate a position of the emitter.

The class of localization techniques of interest in this research is blind localization. With the RSSI information available, power difference of arrival (PDOA) can be used by taking the difference in RSSI between multiple pairs of the sensors, where the results produce common geometrical intersections of circles as the estimated location [2]. Collecting emitter IQ samples at the receiver from the well synchronized sensors allows for the ability to cross-correlate the samples across sensors in the network. The cross-correlation of the received signals results in the difference in time at which each sensor received the signal. The time-difference results produces common geometrical intersections of multiple hyperbolas as the estimated position. This technique is known as time-difference of arrival (TDOA). Other techniques exist to estimate the position of an emitter such as frequency-difference of arrival (FDOA), which is useful for purposes of estimating the position of a fast-moving target and angle-of-arrival (AOA) when antenna-arrays are available for the sensors [5].

For this research, two localization algorithms were studied in detail: Power-difference of arrival (PDOA) and Time-difference of arrival (TDOA). The sensor network design consisted of a star topology where a fusion node is used to triangulate the location of an unknown emitter. The localization algorithms were tested in simulation through MATLAB, emulation through use of the RF environment channel emulator, and multiple field-test scenarios. The accuracy of the geolocation of the emitter was measured under a variety of channel conditions and constraints. This report documents the details of the PDOA and TDOA localization algorithms, explains the various approaches used to develop the geolocation scenarios, and also explains the procedure, results and implications of each experiment executed throughout the study.

Manuscript approved January 3, 2018

2. POWER DIFFERENCE OF ARRIVAL

Consider a number of transceivers distributed spatially over some area of operations (AO). Their goal is to locate a target emitter transmitting at a constant but unknown power P_T from some unknown location denoted (x_T, y_T). All of the sensors as well as the emitter are assumed to be at the same altitude, so the sensors are tasked only with measuring its own location and the RSSI at particular frequencies in the spectrum. The network architecture is shown in Fig. (1).

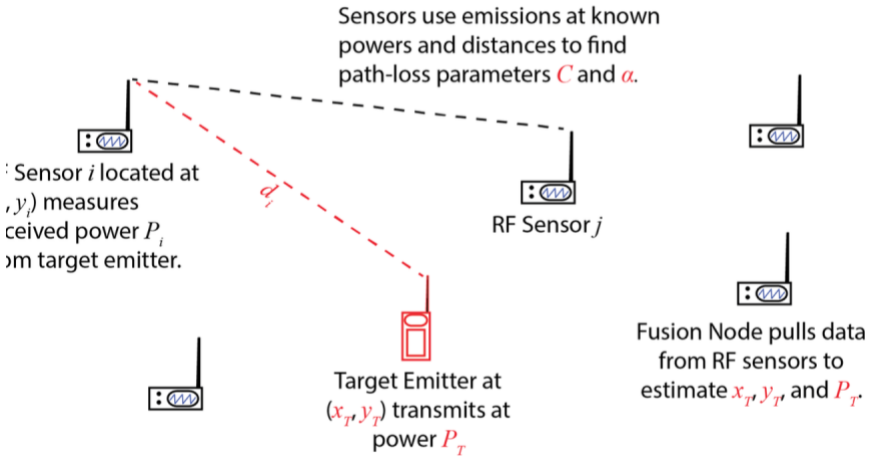

Fig. 1 — An abstraction of the geolocation system. Quantities in red are not known and must be estimated

The path loss is modeled as an exponential function of the distance d_i between the target emitter and the receiving sensor. That is, the received signal power is proportional to d_i^{-a}, where a is initially unknown path loss exponent, usually 2 for a free-space path-loss environment. The constant of proportionality C is also unknown, so both C and a are estimated during sensor network initialization. A system of N equations exists, where N is the number of sensors. The dB path loss expression used in the localization algorithm is shown in (1)

$$\hat{P}_i = \hat{C} - 10\alpha \log(d_i) + \hat{P}_T \qquad (1)$$

For PDOA, a minimum of three sensors is needed to estimate the location of an emitter. From the path loss, the difference in the received power between two sensors in shown in (2).

$$\hat{P}_i - \hat{P}_j = 10\alpha \log\left(\frac{d_j}{d_i}\right) \qquad (2)$$

The power difference and sensor location measurements result in a total of N circles with a maximum of $N*(N-1)$ intersections between the circles. The derivation of the equations of these circles from the given power-difference measurements are described in [2]. We define $q_{ij} = 10^{(P_i - P_j)/10a}$. The sensor coordinates are defined as (x_i, y_i) and (x_j, y_j) respectively. $P_i - P_j$ is the power-difference between the received signal strength of two sensors. With the measurements from two sensors i and j, we are able to find the radio of distances from the two sensors to the target without knowing P_T. This constraint of the location along a set of points on a circle is called the Circle of Apollonius [7].

The equations for the Circle generated by power-difference measurements are shown in (3). These equations are vectorized for purposes of the experiment described later on in this report (Section 6 – PDOA Error Analysis).

$$\begin{aligned} \mathbf{C}_{ij} &= \frac{q_{ij}^2 \mathbf{x}_j - \mathbf{x}_i}{q_{ij}^2 - 1} \\ R_{ij} &= q_{ij} \frac{|\mathbf{x}_j - \mathbf{x}_i|}{|q_{ij}^2 - 1|} \end{aligned} \tag{3}$$

Within Figure (2), each pair of circles yields a true point in the cell with an "X" and a false point in some other cell. A network of *N* sensors in a low-noise channel produces N*(N – 1) intersection points. In the event that there is no intersection between two circles, the midpoint of the shortest line-segment between the two circles is chosen as an intersection. In a theoretical no-noise scenario, all of the circles will have one common intersection point, which is equal to the actual location. For a realistic scenario, where the measurements are not perfect, the intersections tend to converge around the actual location, so a grid-search algorithm is used to find a small area where most of the intersection points lie.

With the circle intersections found, a grid-density algorithm is used. The grid-search process overlays a configurable number of cells on the area of interest once all the intersections are determined. In this research, a 4x4 grid cell was used. The goal is for the cells to be large enough that the intersections corresponding to the true location easily fall into one cell but small enough such that localization of the emitter to a single cell meets the desired spatial resolution. Once the grid is created, the search algorithm finds the grid cell with the highest number of intersections. In the event two or more grid cells have the same number of intersections, the number of intersections in all adjacent cells break a tie. From the selected cell the intersections within the cell are averaged to find the final estimate of the target emitter's location. An illustration of the grid density of Apollonian circle intersections is shown in Fig. (2).

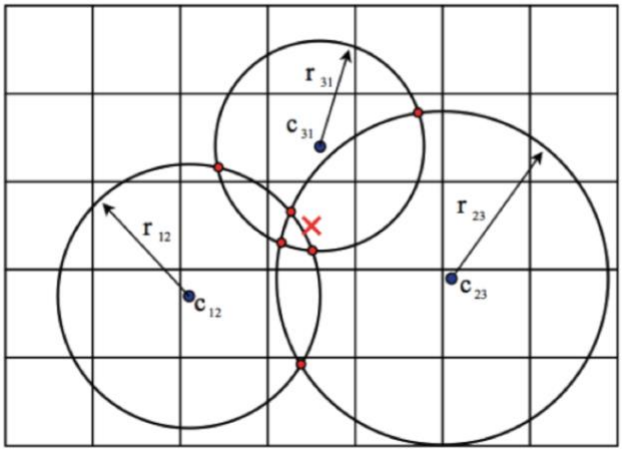

Fig. 2 — The grid search algorithm concludes that the cell with the highest number of intersection points contains the emitter. It then averages the locations of the intersections within that cell to estimate the location of the emitter.

3. TIME DIFFERENCE OF ARRIVAL

The TDOA algorithm locates an emitter source using the intersection of hyperbolic curves generated by cross-correlating IQ data from sensors. Unlike PDOA, which uses RSSI, the TDOA algorithm collects IQ samples from sensors and cross-correlates the IQ data for each pair of sensors to determine the time-difference between the arrival of the emitter signal at each sensor pair. The technique used in this research is an approximation of the maximum likelihood (ML) estimator described in [4]. Applications of the TDOA algorithm are beneficial for environments with high-noise and high-bandwidth emitters, such as radar [5].

The time-difference between the emitter and two sensors will generate a hyperbola and a third sensor will generate another hyperbola. The intersection between the hyperbolae is used as the estimated emitter position [4]. Using a network architecture similar to the one depicted in Fig. (1), the distance between the sensor and actual emitter is $r_i^2 = (x_i - x)^2 + (y_i - y)^2 = K_i - 2yy_i + x^2 + y^2$, for all i = 1, 2, … *M*, where

$$K_i = x_i^2 + y_i^2 \tag{4}$$

If *c* is the signal propagation speed (assumed to be equal to the speed of light) and one of the sensors is selected as a reference sensor (sensor 1) with coordinates (x_1, y_1) and $d_{i,1}$ is the time-difference between sensor *i* and the reference sensor, then

$$r_{i,1} = cd_{i,1} = r_i - r_1 \tag{5}$$

For the case of three sensors, a closed-form solution exists. With three sensors, *x* and *y* can be solved in terms of r_1 in (6) as follows:

$$\begin{bmatrix} x \\ y \end{bmatrix} = -\begin{bmatrix} x_{2,1} & y_{2,1} \\ x_{3,1} & y_{3,1} \end{bmatrix}^{-1} \times \left\{ \begin{bmatrix} r_{2,1} \\ r_{3,1} \end{bmatrix} r_1 + \frac{1}{2} \begin{bmatrix} r_{2,1}^2 - K_2 + K_1 \\ r_{3,1}^2 - K_3 + K_1 \end{bmatrix} \right\} \tag{6}$$

Inserting this intermediate result into (4) at $i = 1$ gives a quadratic in r_1. Substitution of the positive root back into (6) produces the solution, which is used as the emitter estimate. In the event that there is more than one positive root, the ambiguity is resolved by restricting the emitter to a specific area of interest, where the general direction of the emitter is known.

For the case of four or more sensors, the system is over-determined as the number of measurements is greater than the number of unknowns. In the presence of noise, similar to the PDOA case, a set of equations will not intersect at the same point. Let $z_a = \left[z_p^T, r_1 \right]^T$ be the unknown vector, where $z_p = \left[x, y \right]^T$. The solution to the system involves imposing the known relationship (4) to the computed result via another LS computation, which is a two-step procedure and is an approximation of the true ML estimator for emitter localization. The ML estimate of z_a is as follows,

$$z_a \approx \arg\min \left\{ \left(h - G_a z_a \right)^T \psi^{-1} \left(h - G_a z_a \right) \right\} = \left(G_a^T \psi^{-1} G_a \right)^{-1} G_a^T \psi^{-1} h \tag{7}$$

where G, h and j are defined as follows.

$$h = \frac{1}{2}\begin{bmatrix} r_{2,1}^2 - K_2 + K_1 \\ r_{3,1}^2 - K_3 + K_1 \\ . \\ r_{M,1}^2 - K_M + K_1 \end{bmatrix} \quad G_a = -\begin{bmatrix} x_{2,1} & y_{2,1} & r_{2,1} \\ x_{3,1} & y_{3,1} & r_{3,1} \\ . & . & . \\ x_{M,1} & y_{M,1} & r_{M,1} \end{bmatrix} \quad j = h - G_a z_a^0 \qquad (8)$$

The expression in (7) is the generalized least-squares solution of (8). For this research, the source is assumed to be far-away so an approximation of (7) is found and expressed in (9), the explanation is described in [4].

$$z_a = (G_a^T Q^{-1} G_a)^{-1} G_a^T Q^{-1} h \qquad (9)$$

The elements of z_a can be expressed as follows, where e_1, e_2, and e_3 are the estimation errors of z_a

$$z_{a,1} = x^0 + e_1, z_{a,2} = y^0 + e_2, z_{a,3} = r_1^0 + e_3 \qquad (10)$$

Subtracting the first two components by x_1 and y_1 and then squaring the elements leads to another set of equations.

$$\varphi' = h' - G_a' z_a' \qquad (11)$$

where h', G_a' and z_a' are defined as follows.

$$h' = \begin{bmatrix} (z_{a,1} - x_1)^2 \\ (z_{a,2} - y_1)^2 \\ z_{a,3}^2 \end{bmatrix}, G_a' = \begin{bmatrix} 1 & 0 \\ 0 & 1 \\ 1 & 1 \end{bmatrix}, z_a' = \begin{bmatrix} (x - x_1)^2 \\ (y - y_1)^2 \end{bmatrix} \qquad (12)$$

The overall solution and position estimate is obtained from z_a' and is defined as follows. The correct solution is the solution that lies within the particular area of interest.

$$z_p = -\sqrt{z_a'} + \begin{bmatrix} x_1 \\ y_1 \end{bmatrix} \text{ or } z_p = \sqrt{z_a'} + \begin{bmatrix} x_1 \\ y_1 \end{bmatrix} \qquad (13)$$

4. APPROACH

4.1 Simulation

The first stage in researching the algorithms involved simulation through MATLAB. One of the experiments, referred to in section 3.2 used MATLAB™ exclusively. Prior to RFnest emulation, all the implementations of algorithms were tested and debugged using MATLAB. For simulation of PDOA results, the goal was to simulate a channel model in MATLAB. The ideal case of a noiseless channel was first applied, and the path-loss model used was the same one defined in (1), which assumes a log-distance path-loss model. To create a more realistic channel, Additive White Gaussian Noise (AWGN) was added to the path-loss model to simulate the effects of environmental noise. The controllable parameters of the AWGN are the magnitude of the average noise floor and the variance of the sensor measurements due to the noise-floor.

For TDOA due to the error in time-synchronization, the time-difference measurement can have a significant deviation from the actual time-difference. The AWGN was also added to the time-of-arrival measurements, which are calculated by the theoretical equation for propagation speed being equal to distance divided by time, where the speed of propagation is equal to the speed of light.

4.2 Emulation

It is useful to produce a network prototype that can be fully tested and debugged in a controlled laboratory environment with a channel emulator prior to field testing. Central to the RF wireless network environment emulator (RFNWEE) is the RFnest D512 series. This allows the user to control channel properties such as propagation loss, delay, Doppler effect, multipath, and fading profiles. Other components of the lab setup consist of GPS simulators and real-time spectrum analyzers (RSAs). The radios used in the research are Universal Software Radio Peripherals (USRPs), which run using GNU radio software on a computer connected to the USRP. The architecture of the RFNWEE is shown in Fig. (3) and a picture of the DSA lab setup at NRL is shown in Fig. (4).

The RFnest consists of twelve bidirectional nodes. The radio under test (RUT) is interfaced with the D512 through the RF daughterboard within the RFnest, which converts RF to IF bands for signal processing. The digital daughterboard (DDB) interfaces with the RFDB and main FPGA of the emulator. The channel emulation properties utilize the tapped delay line within the DDB. A network of computers is integrated to execute emulation for scenarios and radio operations. The servers are connected into a local network via switches and patch panels, for purpose of running emulations remotely. More details of the RFWNEE and corresponding experiments can be found in [1]. The RFWNEE GUI is shown in Fig. (5)

The advantage of using the RFNWEE for this work allows for repeatability, realism, cost and time saving and is used as an important first step to preparation for the field test.

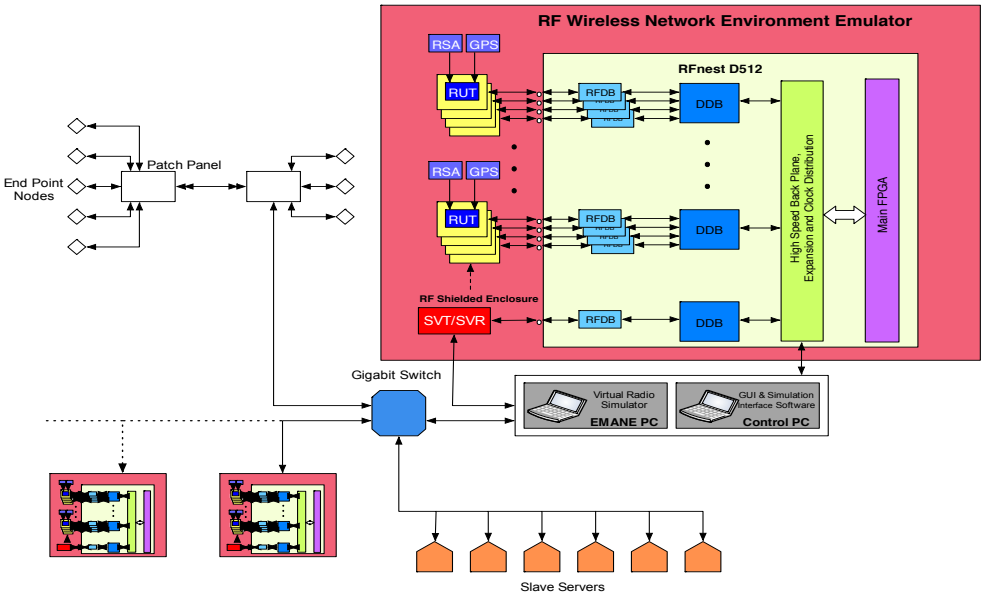

Fig. 3 — RFWNEE Architecture

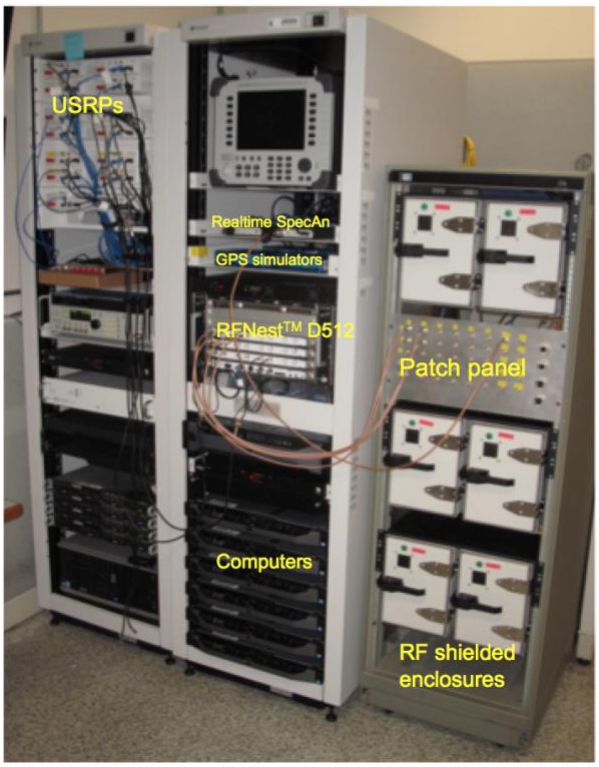

Fig. 4 — RFWNEE Lab Setup

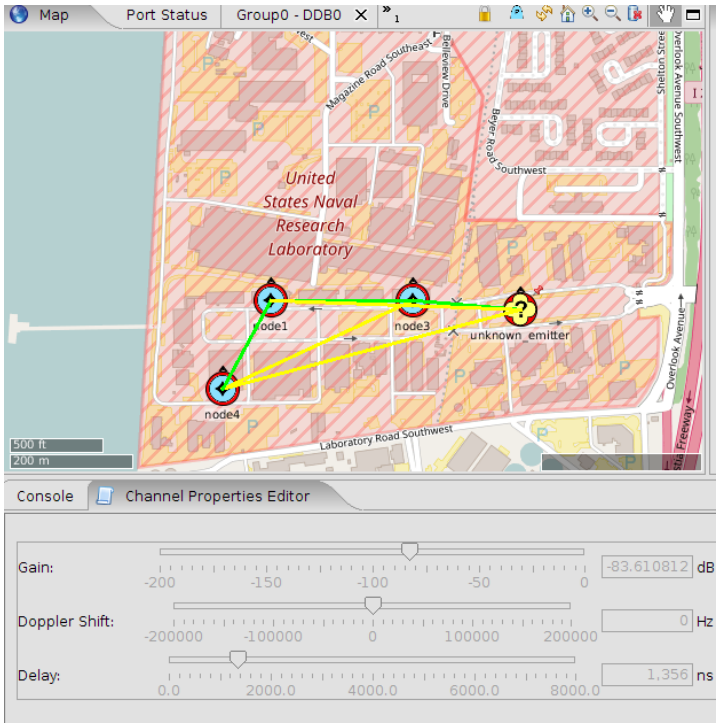

Fig. 5 — RFWNEE Channel Emulation GUI. The path-loss parameters can be controlled manually or automatically based on a particular path-loss model

4.3 Field Testing

Field testing the sensor network technology was a final and important step toward assessing the performance of the geolocation sensor network. All experiments utilized the star topology referred to in Fig. (1). The programming language used to create the platforms was Python, because of its ability to use GNU radio blocks and start sampling at a specific time, which was particularly important for TDOA synchronization.

The backhaul communications used to obtain sensor data has differed for each experiment. There were three types of backhauls used throughout the course of the experiment: USRPs communicating, communications over standard wired or wireless Ethernet, and LoRa communication modules. The first type of communications backhaul used the USRPs acting as transceivers. They would collect sensor information from the environment (RSSI or IQ samples), and create their own GMSK modulated packets to be sent to another USRP used exclusively as the fusion radio. The computer connected to the fusion USRP would then read the demodulated packets and localize the emitter with one of the algorithms.

The main purpose of the USRPs was to act as passive sensors, that can detect RSSI or signal IQ samples. A disadvantage to using USRPs for the backhaul communications is the poor receiver sensitivity. Practical geolocation applications require a larger operational range, so a second backhaul employed was the use of WiFi. The WiFi backhaul was used for the TDOA system, where the IQ samples encapsulated in packets was sent over the network using Python scripts. The advantage of this backhaul is that the bit rate and maximum packet sizes are larger, and can send a packet of approximately 10,000 IQ samples. The disadvantage to the WiFi backhaul is its range. In order for packets to be transmitted over larger distances, WiFi extenders are needed, and another disadvantage is security. WiFi in a tactical environment is highly susceptible to intentional interference from an adversary.

The third backhaul is the LoRa WAN protocol. This wireless technology allows for long-range and low-power transmission over the ISM band. The device used was the Microchip RN2903 modem. The receiver sensitivity is around -146 dBm, which enables reception for transmission coverage around 15 km in suburban areas and up to 5 km in urban areas. The disadvantage is the amount of system throughput. The data rate is approximately 100 bps and the maximum packet size is 255 bytes. This backhaul technology has only been used for the PDOA experiment with the mobile emitter, shown in section 3.3. This backhaul has not been field tested with TDOA because of the algorithm throughput requirements needed to compute the location based on IQ samples. Other TDOA methods, such as knowing about the emitter modulation, would allow for a simple time-of-arrival report, which would reduce the required throughput.

5. STATIC SENSOR NETWORK TEST

The purpose of this experiment is to demonstrate the PDOA algorithm in a proof-of-concept field test using a network of GNU radio sensors. The results and field test procedure are found in [3]. The geolocation algorithm would estimate the position of a single emitter at a frequency of 903 MHz transmitting a pure sinusoidal tone at 15 dBm. The USRP sensors were arranged in an enclosed triangular area (three sensors), and square (four/five sensors). This geometry results in an enclosed area of operation (AO) of sensor operation. The emitter was moved to three unique locations (inside AO, along AO boundary, well outside AO), and the PDOA algorithm ran for multiple iterations with the emitter stationary at the particular location. The receiver USRP gains were set to 19 dBm, resulting in a noise floor of -105.65 dBm. From calibration, the path-loss constants were found to be $a = 2.43$ and C = 0.004.

Fig. 6 – Sensor and target placement for field test

The results of the field test found that the position of the emitter relative to the sensors affects the estimated location accuracy. The reason for this is that moving an emitter further away from sensors decreases the received signal strength, resulting in greater noise variance and higher location ambiguity. The plots in Figs. (6) (7) shows the error measured for each iteration and the cumulative average of the error with respect to the overall average. The actual mean error for all three unique locations is found in Table 1. The RFnest results show a higher average error for each since the actual locations of the sensors was spread further apart to further test the limits of the algorithm. To improve accuracy, the path loss could be calibrated for multiple emitter locations versus just one location.

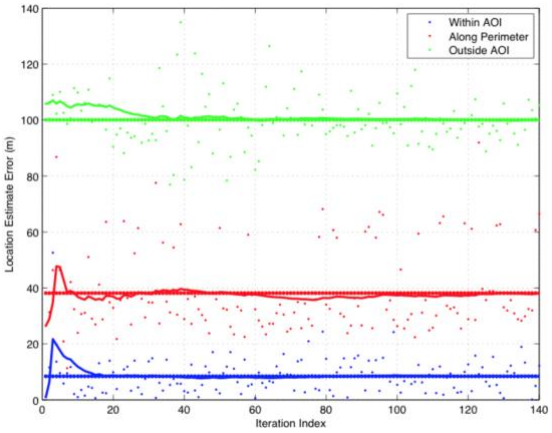

Fig. 7 — Field Test Result

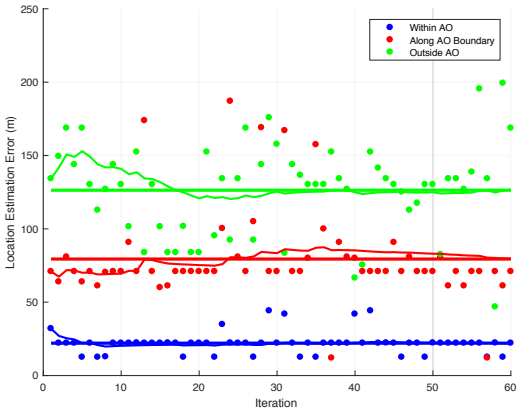

Fig. 8 — RFnest Emulation Result

Table 1 — Static PDOA Test (Estimation Accuracy)

Scenario	Field Test Error (m)	RFnest™ Error (m)
Within AO	8	22
Along AO Boundary	38	79
Outside AO	100	126

6. PDOA ERROR ANALYSIS

The purpose of this experiment was to quantify the magnitude of error in location estimation based on the location of the emitter with respect to the sensor network. In particular, we analyze sources and magnitudes of errors when using the PDOA algorithm with a group of sensors. We show that the limit where the unknown transmitter is a large distance outside the sensors' area of characteristic length, the error in the emitter's location is amplified by a factor much greater than unity in the estimate of the location. This experiment quantifies the phenomenon wherein the error in the results of PDOA localization is exacerbated as the target is moved further from the sensor network.

The inputs to the PDOA algorithm are the sensors' locations and differences in the received power as measured by these sensors. The emitter power need not be known; so PDOA is useful when a-priori information about the emitter is unknown. The set of possible emitter locations generated by each pair of sensors is a circle. The intersections of these circles are mapped to a 2D grid and a weighted average of the grid locations estimates the location of the target emitter.

Finding Apollonian circles and their intersections is a non-linear process, and it does have significant short-comings regarding accuracy and noise-amplification. Environmental effects such as multipath and fading break the assumption of an invertible function relating received power to the distance between the emitter and sensor. Furthermore, the algorithm can only locate one emitter at a particular frequency and geographic area. It cannot distinguish multiple emitters in the same band.

From the experiment described in Section 5, an important observation was that the algorithm accuracy depended on how close the emitter was to the sensor network. The focus of this experiment is to quantitatively analyze the effect of the emitter being moved further away from the sensor network, area of operation. We employ two-dimensional geometric approximations to show that the non-linearity of the PDOA algorithm aggravates measurement noise. We show that even in the case of perfect channel signal measurement, the PDOA algorithm will amplify sensor location noise to an arbitrarily high level with increasing distance. We calculate the rate at which the errors accumulate and verify the analytical results with simulations.

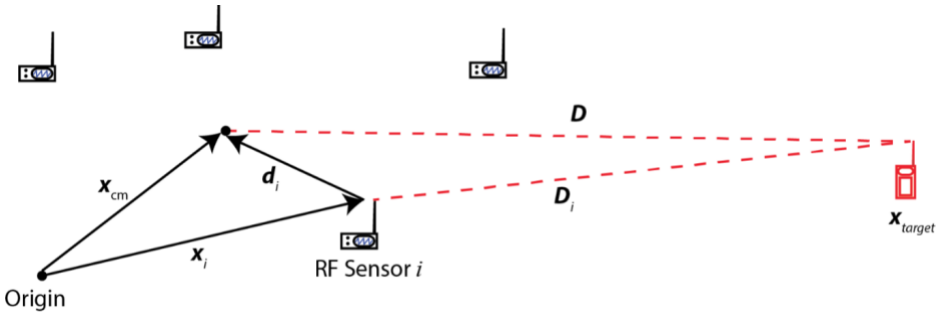

Fig. 9 — A diagram of model geometry

Consider a PDOA situation as in Fig. (9). A group of sensors will locate a transmitter of unknown power at an unknown location x_{target}. Sensor *i* is located at x_i and there exists a point in space at x_{cm} which is much like the center of mass. This point need not actually be the center of mass. D is the vector representing the distance between x_{target} and x_{cm}. D_i is the vector representing the distance between x_{target} and x_i. All we need is a point such that the following relation holds:

$$|\mathbf{D}| >> |\mathbf{d}_i|, \quad " \ i \qquad (13)$$

This is our quantitative way of saying that the target emitter is far outside the sensor area of operations. We assume that some data fusion node uses the PDOA path-loss equations to calculate the distance ratios to the target emitter. That is, for each pair of sensors *i* and *j*, the power-level P_i and P_j is measured at each sensor location, and $P_i - P_j$ is the power-difference between the two sensors. For our application, we use the log-normal path-loss model for position estimation given in (14), where *C* and α are path-loss constants. For this experiment, $\alpha = 2$ and $C = 0.004$. These values represent the approximation of free-space path-loss.

$$P_i = C - 10\alpha \log|\boldsymbol{D}_i| \qquad (14)$$

When taking the power-difference between two sensors, *i* and *j*, the result is as follows,

$$P_i\text{-}P_j = 10\alpha \log \frac{|\boldsymbol{D}_i|}{|\boldsymbol{D}_j|} \qquad (15)$$

As described in Section 2, the quantity q_{ij} is the ratio of the distances between the target emitter and a given sensor, that is defined in (16). In addition, the sensor location incurs a small measurement error and white Gaussian noise is used as the additive error (17).

$$q_{ij} = \frac{|\mathbf{D}_i|}{|\mathbf{D}_j|} \tag{16}$$

$$\tilde{x}_i = x_i + \varepsilon_i \tag{17}$$

The estimate $\widetilde{x_i}$ incurs a measurement error ε_i. We need not define a distribution over this random error just yet, but we shall see that the errors are amplified by the geometric assumption in (13), yielding larger error terms in the overall estimate of x_{target}. We define a perturbation parameter in (18) to quantify how large the error becomes

$$g = \frac{\max_i |d_i|}{|\mathbf{D}|} \ll 1 \tag{18}$$

The PDOA algorithm entails the determination of an Apollonian circle for each pair of sensors. On a 2-dimensional plane, the target lies somewhere on the circle (with center $\mathbf{C}_{ij}$ and radius R_{ij}) of every pair of sensors. If there were no measurement errors ($\varepsilon_i = 0$ for all i and j), then the estimates of these circles' radii and centers would be exactly correct. However, the errors yield estimated circle parameters $\widetilde{C_{ij}}$ and $\widetilde{R_{ij}}$ that are corrupted by noise. The equations for the centers and radii are defined as follows,

$$\tilde{\mathbf{C}}_{ij} = \frac{q_{ij}^2 \tilde{\mathbf{x}}_j - \tilde{\mathbf{x}}_i}{q_{ij}^2 - 1} = \mathbf{C}_{ij} + \frac{q_{ij}^2 \boldsymbol{\varepsilon}_j - \boldsymbol{\varepsilon}_i}{q_{ij}^2 - 1} \tag{19}$$

$$\tilde{R}_{ij}^2 = \left| \frac{q_{ij}}{q_{ij}^2 - 1} \right|^2 \left| \tilde{\mathbf{x}}_j - \tilde{\mathbf{x}}_i \right|^2 = R_{ij}^2 + \left| \frac{q_{ij}}{q_{ij}^2 - 1} \right|^2 \left(\left| \boldsymbol{\varepsilon}_j - \boldsymbol{\varepsilon}_i \right|^2 + 2 \left(\mathbf{x}_j - \mathbf{x}_i \right) \cdot \left(\boldsymbol{\varepsilon}_j - \boldsymbol{\varepsilon}_i \right) \right) \tag{20}$$

Let us express the error terms on the right-hand sides of (19) and (20) in terms of the perturbation parameter. We do this by expressing the distance ratio for a pair of sensors explicitly separating out the part that is of order γ^2. Letting $\boldsymbol{d_i} = d_i \widehat{\boldsymbol{d}_i}$ and $\boldsymbol{D} = D\widehat{\boldsymbol{D}}$ for unit-vectors $\widehat{\boldsymbol{d}_i}$ and $\widehat{\boldsymbol{D}}$, we have,

$$\frac{|\mathbf{D}_i|}{|\mathbf{D}_j|} = \frac{|\mathbf{D} + \mathbf{d}_i|}{|\mathbf{D} + \mathbf{d}_j|} = 1 + \frac{d_i}{D} \hat{\mathbf{D}} \cdot \hat{\mathbf{d}}_i - \frac{d_j}{D} \hat{\mathbf{D}} \cdot \hat{\mathbf{d}}_j + O[\gamma^2] \tag{21}$$

Putting this simplification into our expression for $q_{ij,}$ we have,

$$\begin{aligned} q_{ij} &= 1+\frac{d_i}{D}\hat{\mathbf{D}}\cdot\hat{\mathbf{d}}_i-\frac{d_j}{D}\hat{\mathbf{D}}\cdot\hat{\mathbf{d}}_j+O[\gamma^2] \\ q_{ij}^2 &= 1+2\left(\frac{d_i}{D}\hat{\mathbf{D}}\cdot\hat{\mathbf{d}}_i-\frac{d_j}{D}\hat{\mathbf{D}}\cdot\hat{\mathbf{d}}_j\right)+O[\gamma^2] \\ &= 1+H+O[\gamma^2] \end{aligned} \tag{15}$$

where $H=H(\boldsymbol{D},d_i,d_j)$ is a function of the distances relative to the reference point x_{cm}. Note that $|H| << 1$ as a consequence of (13). In terms of these new variables, the circle parameter estimates in (19) and (20) can be rewritten as follows.

$$\tilde{\mathbf{C}}_{ij}=\mathbf{C}_{ij}+\boldsymbol{\varepsilon}_j+\frac{1}{H}(\boldsymbol{\varepsilon}_j-\boldsymbol{\varepsilon}_i) \tag{16}$$

$$\tilde{R}_{ij}^2=R_{ij}^2+\left(\frac{1}{H^2}+\frac{1}{H}\right)\left(\left|\boldsymbol{\varepsilon}_j-\boldsymbol{\varepsilon}_i\right|^2+2\left(\mathbf{x}_j-\mathbf{x}_i\right)\cdot\left(\boldsymbol{\varepsilon}_j-\boldsymbol{\varepsilon}_i\right)\right) \tag{17}$$

From (16) and (17), the terms such as 1/H and $1/H^2$ dominate. So, what should be expected is for the error for most of the circle terms to increase with respect to the change in H.

Given the expression for the circle center in (16), we can rearrange the equation by taking the magnitude of both sides, since the error is associated with the magnitude (distance from the actual circle center to the estimated circle center). We then take the expected value of both sides so that we obtain a linear equation shown in (18), which is dependent on the expected value of ε_i and ε_j with a slope that is dependent on H, which varies with the distance of the emitter from the sensor network. Thus, we can show that the variance of the error will increase by a factor inversely proportional to H^2.

$$E[|\tilde{\mathbf{C}}_{ij}-\mathbf{C}_{ij}|]=\frac{1}{H}E[(|(H+1)\boldsymbol{\varepsilon}_j-\boldsymbol{\varepsilon}_i|] \tag{18}$$

Similarly, the expected value of the circle radius error is found in (19).

$$E[\tilde{R}_{ij}^2-R_{ij}^2]=\left(\frac{1}{H^2}+\frac{1}{H}\right)E\left[\left|\boldsymbol{\varepsilon}_j-\boldsymbol{\varepsilon}_i\right|^2+2\left(\mathbf{x}_j-\mathbf{x}_i\right)\cdot\left(\boldsymbol{\varepsilon}_j-\boldsymbol{\varepsilon}_i\right)\right] \tag{19}$$

Rearranging the equations into this form allows us to verify the relations using a sufficiently large sample size for a simulation to calculate the expected value and variance of error.

To find the intersection between circles, we use a coordinate independent system by letting two circles be represented by $|\boldsymbol{X}\text{-}C_i|^2=R_i^2$ for i = 0, 1 where i represents a particular circle. We define $U=C_1\text{-}C_0$ and $V=U^{\perp}$. The intersection points can be written in the form as shown in (20).

$$\boldsymbol{X}=\boldsymbol{C_0}+s\boldsymbol{U}+t\boldsymbol{V} \tag{20}$$

The equation for *s* and *t* are shown in (21) and (22).

$$s = \frac{1}{2}\left(\frac{R_0^2 - R_1^2}{|\boldsymbol{U}|^2} + 1\right) \tag{21}$$

$$t^2 = \frac{R_0^2}{|\boldsymbol{U}|^2} - s^2 \tag{22}$$

Expanding these equations to obtain the first-order term plus the error is difficult, so rather than using the same method for the center and radii, we inspect the terms according to their orders of magnitude. Looking at *s*, both the numerator and denominator are on the order of $1/H^2$, which means *s* is close to unity. Similarly, *t* is also close to unity. From (20) it is clear that the error in **X** is on the order of 1/H, so we should expect to see the value of error increase linearly.

To verify the analytical results of the PDOA error analysis, MATLAB™ was used to simulate the error for the circle centers, radii, intersections, and overall error in target estimation as the emitter is moved further outside the area of sensor operation. The locations of the sensors were arbitrarily chosen and the center of mass of the sensors was chosen as the reference point for the model geometry. At each emitter location, the ratio of the distance of the emitter and the furthest sensor from the center of mass was taken and at each of these points, the PDOA algorithm was performed at a given emitter location for $n = 1000$ iterations with ε_i and ε_j changing each time. Of the data (center and radii) generated by each iteration, the expected value and variance of the result is taken. The variance in terms of ε_i and ε_j, ranges from 1 to 10. Three locations of the emitter were chosen at 10, 20 and 30 kilometers from the network reference point respectively.

Figure 10 instances show the results of the expected error value of circle radii and centers as well as intersections and overall location estimation error over the entire emitter path extending outward from the sensor area of operation. In addition to the plot of experimental error, the slope of each line was calculated according to the formula for H. The equation for H can be rewritten as follows.

$$H = 2\left(\frac{d_i}{D}\hat{\mathbf{D}} \cdot \hat{\mathbf{d}}_i - \frac{d_j}{D}\hat{\mathbf{D}} \cdot \hat{\mathbf{d}}_j\right) \tag{23}$$

From (23), it follows that H is dependent on the distance of the emitter from the sensor network, where the sensors distance from the reference point are fixed. The values of H were calculated for each of the three distances and the slopes were calculated from (18) and (19) to give the theoretical slope.

The plots shown in Fig. (10) illustrate the slope of the line with theoretical data (solid line) compared to that of the experimental data (box-plot). From Fig. (10a) and Fig. (10b), the experimental mean or expected value of error for both the center and radii of an Apollonian circle is close to that of the theoretical expected value using the equation derived from the previous section. This shows that the simulated graphical results and the analytical equations derived are consistent. Similarly, it is shown from the box-plot that an increase in expected value of error will also correspond to an increase in the variance of the error of the Apollonian circle terms.

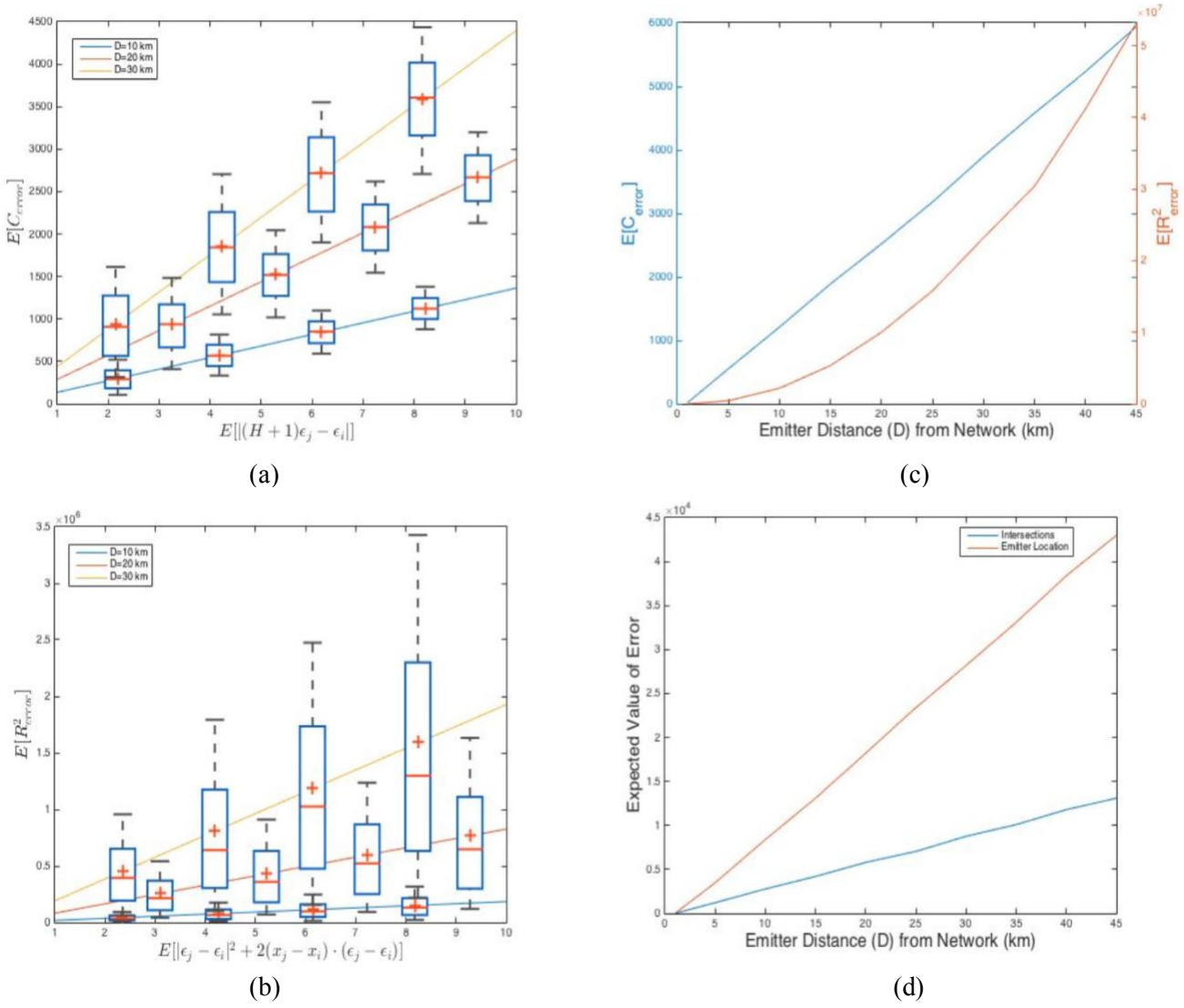

Fig. 10 — (a) Expected value of circle center error as a function of expected value of sensor noise. (b) Expected value of circle radii error as a function of expected value of sensor noise. (c) Expected value of error in Apollonian circle centers and radii as a function of distance of the emitter from the sensor network (d) Expected value of overall location error as a function of distance from the network

In addition to verifying the analytical Apollonian circle perturbation equations, the effect on the accuracy of the algorithm of emitter distance from the sensor network was also simulated. A range of emitter distances was chosen ranging from 1 kilometer to 45 kilometers from the reference point. At each distance, the average error over n = 1000 iterations of PDOA algorithm was calculated at each distance for circle centers, radii, and intersections. The overall expected error of the estimated emitter location was also computed to demonstrate that errors in the Apollonian circle parameters accumulate, leading to an overall effect on the accuracy of the algorithm. Fig. (10c) shows the expected value of error for circle radii and centers. As expected, since the error in the center increases on the order of 1/H, the relationship should be linear and for the radii, the relationship should be quadratic as the error increases on the order of $1/H^2$.

The plot in Fig. (10d) shows the expected error for circle intersections and the overall location estimation. While it is difficult to mathematically analyze the error in overall location, it is expected to be linear since it should correspond to error in the intersections, which also increases on the order of 1/H.

From these results, it is clear that the variance and expected value of error is amplified for all of the terms (centers, radii, and intersections) and the overall estimation error, the further the emitter is moved away from the area with respect to the center of mass of the sensors. These results support the finding of the analytical expressions of noise amplification linearity in all of the terms with respect to H. An important finding is that the analytical results do not support intuition that in a noisy environment, the noise should help to improve accuracy in some instances. The reason for the dominance of error in the algorithm arises from the noise terms being collected in the non-linear expressions for the circle centers and radii.

For a practical implementation of a sensor network, the sensor RSSI is not noise-free, so for a separate analysis, we now assume that some noise is added to the received power of a sensor. A modified equation (16) now has a noise term η_{ij} added and we rewrite the equation as follows.

$$q_{ij} = \frac{|\mathbf{D}_i|}{|\mathbf{D}_j|} + \eta_{ij} \tag{24}$$

To find an expression for the modified terms for center and radii, we assume $\eta_{ij} << 1$ and $H << 1$. The expression for the modified circle center is rewritten in (25)

$$\tilde{\mathbf{C}}_{ij} = \frac{(1+2H)\mathbf{x_j} - \mathbf{x_i}}{2(H+\eta_{ij})} \tag{25}$$

If $H >> \eta_{ij}$, then $\frac{1}{2\left(H+\eta_{ij}\right)}$ can be approximated as $\frac{1}{2H}\left(1-\frac{\eta_{ij}}{H}\right)$. Rewriting the center in terms of its first order plus the perturbation terms, the equation is rewritten in (26)

$$\tilde{\mathbf{C}}_{ij} = \mathbf{C_{ij}} + \frac{1}{2H}\left(1-\frac{\eta_{ij}}{H}\right)(\varepsilon_\mathbf{j} - \varepsilon_\mathbf{i}) \tag{26}$$

The slope of the linear equation is now affected by the scalar $\left(1-\frac{\eta_{ij}}{H}\right)$. If the absolute value of this term is between zero and one, then the slope of the error function will be reduced. However, this is not always guaranteed as the sign of η_{ij} and H have an equal chance of being positive and negative. While noise in power readings can sometimes help to reduce the location error due to sensor position noise, it is equally likely that it can exacerbate the error as well.

7. PDOA MOBILE EMITTER FIELD TEST

The purpose of this experiment was to measure the performance of PDOA algorithm with a mobile emitter traveling different combinations of paths and different sensor topologies. While the previous field test demonstrated how PDOA performs under more friendly sensor topologies and a fixed emitter, several of the emitter paths contain hostile conditions that are more realistic, such as obstruction of line-of-sight by buildings and irregular sensor topologies. A vehicle was used to drive the emitter USRP around NRL. For this experiment, the emitter consisted of a USRP N210 transmitting AM and FM signals. These two modulations were used to determine if there was any correlation between the modulation and the algorithm accuracy.

For this experiment, three different sensor topologies were chosen: a linear topology over a small area of operation (short linear), a linear topology over a larger AO (long linear), and a triangular topology. Three different emitter paths were also chosen and are shown in Fig. (11). The first path is a path around the NRL mall (orange path), with the least amount of obstruction to the line-of-sight. The second and third paths are the river (blue path) and partially obstructed path (green path), in which part of the path involves the mobile emitter vehicle driving behind building out of sight of most to all of the sensors.

Fig. 11 — Google earth shows the three emitter paths: mall loop (orange), river (blue), and partially obstructed (green)

Fig. 12a — Short Linear Topology. (Red icons indicate sensor locations)

Fig. 12b — Long Linear Topology. (Red icons indicate sensor locations)

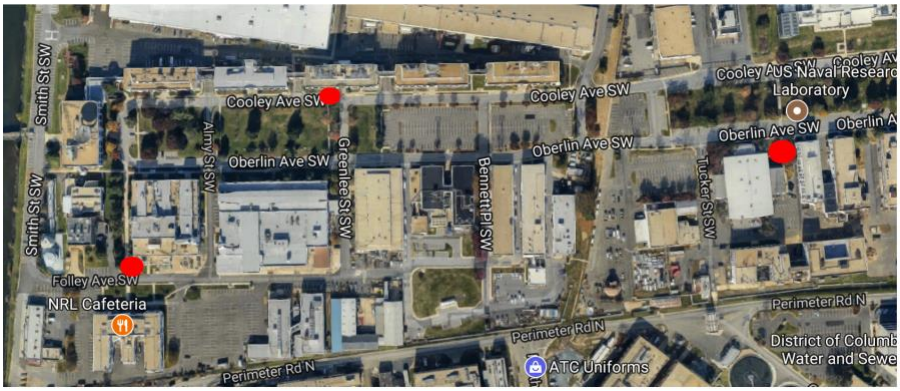

Fig. 12c — Triangular Topology. (Red icons indicate sensor locations)

For the fusion node, the LoRa WAN was used as a backhaul for the sensors to send their data to a computer containing the PDOA processing algorithm. In addition, the fusion node would generate and update a KML file consisting of the real-time locations of all sensors and the latest estimation of the emitter. This Google-Earth interface of the sensor topologies is shown in Fig. (12a-c).

For each scenario, the algorithm's accuracy was calculated by the measured error of all estimated points. Fig. (13a-c) shows three different plots of the accuracy of the location estimation for the three different emitter paths. Each plot contains the error, calculated every 20 seconds over the entire course of the path for each sensor topology.

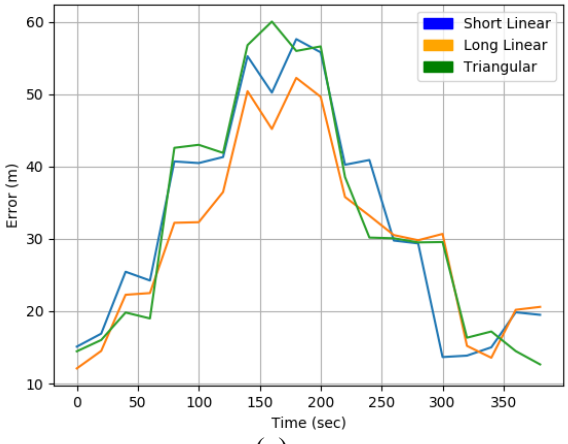

(a)

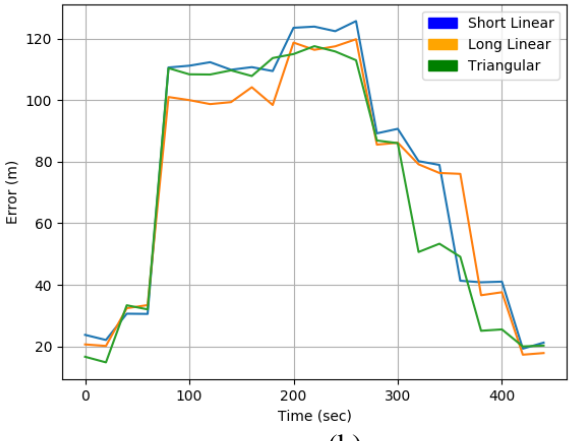

(b)

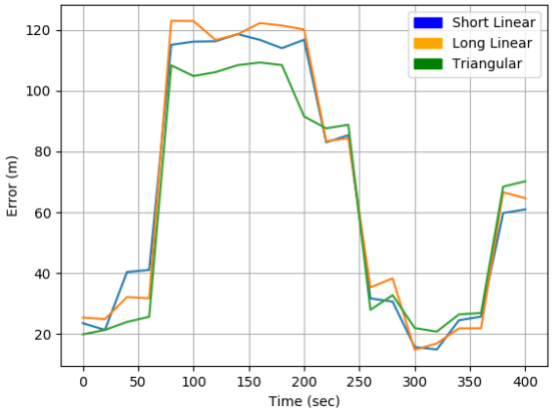

(c)

Fig. 13 — Geolocation estimation error for (a) Mall path (b) River path (c) partially obstructed path

From the results, it is clear that there is a direct correlation between the percentage of accuracy and the average error for each particular scenario. This is to be expected since a larger average RMSE in the distance from the actual emitter to the estimated emitter resulted in fewer measurements being within the 20 m range of tolerance. Some important findings were the large drop-off in accuracy from the mall emitter path to the river and the partially obstructed paths. This significant decrease in performance was due to the emitter being obstructed by more buildings throughout most of the duration of the scenario. Oftentimes, the fusion node was not able to triangulate a position, because the emitter was below the noise floor of -106.65 dBm. One important result was the slight decrease in accuracy from the linear to triangular topologies of the mall path. A triangular topology should be more accurate since there is less ambiguity in the geometry of the Apollonian circle intersections. The reason for the less accurate outcome is that one of the sensors was obstructed from the line-of-sight with the NRL mall, which led to less accurate RSSI measurements for that particular sensor.

8. TDOA EMULATION

For the TDOA measurement to be accurate, the receiver radios should be well synchronized. Utilizing the GPSDO provided in the USRP to receive the GPS signal, the radios are able to be synchronized to a common clock to achieve time-aligned samples on the order of nanosecond resolution. Once all sensors are synchronized, each sensor collects IQ samples. The emitter used in this experiment is a BPSK modulated signal with its data generated using PN23 randomization. BPSK was chosen due to its correlation properties, which is needed to measure the time difference. Each pair of sensor data is cross-correlated to measure this time-difference. The result of the correlation contains a peak in the time-domain, where the peak represents the time-difference between the two correlated sensors. When the data is computed, the position is estimated using the algorithm described in section 1.3. The TDOA system is shown in Fig. (14).

This experiment was performed using the RFWNEE described in section 2.2. Three sensors are used in this experiment, and the emitter was mobile, and traveled the NRL mall loop path similar to the experiment described in section 3.3. The accuracy was evaluated using the same three topologies from the experiment in section 3.2 (short linear, long linear, and triangular).

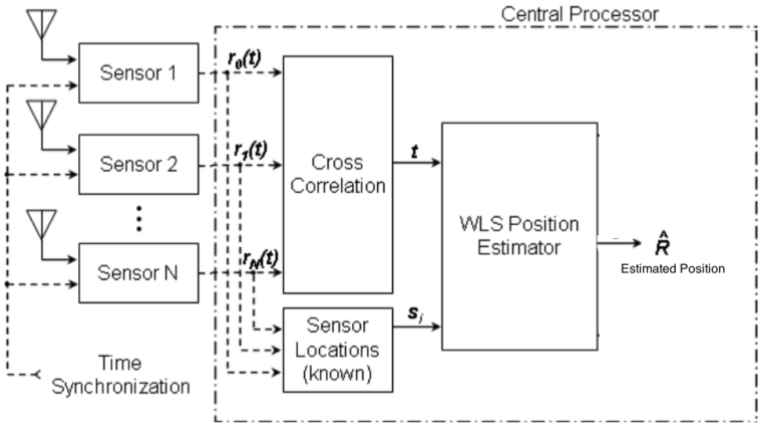

Fig. 15 — Block diagram of TDOA system

The results of the emulation are shown in Table 3. From these, it was found that the short-linear topology had the highest error. This was because since the sensors were spaced closer together, the time-difference between them was smaller. For this experiment, the USRP N210 hardware was used, and the maximum sampling rate was 25 MHz, resulting in a sample resolution of 40 nanoseconds. This lower resolution restricts the accuracy of the time-difference measurement, and as a result the accuracy of the localization algorithm. Another finding was that when the emitter was further away from the sensors, the accuracy was improved, because of larger time-differences to offset the 40-nanosecond resolution.

Scenario	Error (m)
Short-Linear	37.2
Long-Linear	26.8
Triangular	31.0

9. CONCLUSIONS

The experiments conducted have given valuable insight into the various methods of emitter localization and the practicality of different network technologies used for a geolocation system. We have tested with multiple sensor configurations, mobile emitter paths, and obtained results for a variety of target signals, continuous waveforms and analog and digital modulations. Two of the algorithms studied: TDOA and PDOA and their associated experiments demonstrated important trends in sensor geometry with respect to the target emitter. Through simulation, emulation and field-testing, it was found that in PDOA, the further an emitter is away from the sensor network, the larger the error. This trend was not present in TDOA due to its noise-resilience. While PDOA has been field tested, potential future work would relate to studying field test implementations of TDOA, using LoRa backhaul to implement a coastal-monitoring sensor network to track ship radar or other commercial signals of interest. Other potential future work is using more detailed path-loss models to track emitters in an urban environment with increased accuracy.

REFERENCES

1. M. Dillon, E.H. Fu, D. Gdula, T. Mai, J. Molnar, and L. Tran, *Real and Virtual Wireless Radio Network Emulator,* Military Communications Conference (IEEE, 2016). doi:10.1109/MILCOM.2016.7795507

2. S. Guo, B. Jackson, S. Wang, R. Inkol, and W. Arnold, "A novel density-based geolocation algorithm for noncooperative radio emulator using power difference of arrival", *SPIE Defense, Security and Sensing,* vol. 8061, (May 2011).

3. A. Robertson, M. Dillon, S. Kompella, E.H. Fu, D. Perkins, and J. Molnar, "Distributed trasnsmitter localization by power difference of arrival on a network of radio sensors", Naval Research Laboratory Networks and Communications Branch, NRL/MR/5524—15-9576 (February 3, 2015).

4. Y.T. Chan, "A simple and efficient estimator for hyperbolic location", *IEEE Transactions on Signal Processing* Vol. 42, (August 1994).

5. D. Musicki, W. Koch, "Geolocation using TDOA and FDOA Measurements", Entropy Data Pty Ltd, Wachtberg, Germany. *11th International Conference on Information Fusion*, (July, 2008).

6. S. Ravindra, S.N. Jagadeesha, "Time of Arrival Based Localization in Wireless Sensor Networks: A Linear Approach", Jawaharlal Nehru National College of Engineering, Visvesvaraya Technological University, Belguam, Karnataka, India. *Signal and Image Processing: An International Journal* Vol. 4, (August 2013).

7. J. Cox, M.B. Partensky "Spatial localization problem and the circle of Apollonius", *arXiv preprint physics/0701146* (2007)